Global Distribution and Interannual Variation in the Winter Halocline

HIROMICHI UENO,[a] MASATO ODA,[b] KATSURA YASUI,[b] RYO DOBASHI,[a] AND HUMIO MITSUDERA[b,c]

[a] *Faculty/Graduate School of Fisheries Sciences, Hokkaido University, Hakodate, Japan*
[b] *Graduate School of Environmental Science, Hokkaido University, Sapporo, Japan*
[c] *Institute of Low Temperature Science, Hokkaido University, Sapporo, Japan*

(Manuscript received 13 March 2021, in final form 9 December 2021)

ABSTRACT: The distribution and interannual variation in the winter halocline in the upper layers of the World Ocean were investigated via analyses of hydrographic data from the World Ocean Database 2013 using a simple definition of the halocline. A halocline was generally observed in the tropics, equatorward portions of subtropical regions, subarctic North Pacific, and Southern Ocean. A strong halocline tended to occur in areas where the sea surface salinity (SSS) was low. The interannual variation in halocline strength was correlated with variation in SSS. The correlation coefficients were usually negative: the halocline was strong when the SSS was low. However, in the Gulf of Alaska in the northeastern North Pacific, the correlation coefficient was positive. There, halocline strength was influenced by interannual variation in Ekman pumping.

KEYWORDS: Ocean; Salinity; Interannual variability

1. Introduction

A halocline is a layer containing a strong vertical salinity gradient. This layer may include a pycnocline, particularly at high latitudes, separating the surface and subpycnocline waters (Fiedler and Talley 2006). The halocline has a significant impact on physical and biogeochemical processes in the World Ocean. For example, low-salinity surface waters and the associated strong halocline in the northern North Pacific are thought to prevent sinking of surface water to great depth in that region (Warren 1983; Emile-Geay et al. 2003). Menviel et al. (2012) performed experiments using an Earth system model in which a negative freshwater flux was imposed in the northern North Pacific, the halocline vanished, and a deep Pacific meridional overturning circulation was established. They reported that nutrient concentrations in the euphotic zone increased by about 25% globally, leading to a 20% increase in global export production and highlighting the importance of the halocline to physical and biogeochemical processes.

Previously, salinity stratification, including the halocline, has been studied from the viewpoint of the barrier layer. This is the layer between the halocline in the surface isothermal layer and the thermocline located underneath, and plays a significant role in determination of mixed layer depth, particularly in tropical and subtropical regions (Sprintall and Tomczak 1992). This layer influences heat and momentum exchanges between the atmosphere and the ocean and thus has an impact on air-sea interaction (Vialard and Delecluse 1998; Masson et al. 2004). Sprintall and Tomczak (1992) investigated the barrier layer in tropical and subtropical regions and found that the layer is formed by subduction of saline water or by strong rainfall and river runoff. Study of the barrier layer was extended to the world oceans, for example by Tomczak and Godfrey (1994), de Boyer Montégut et al. (2007), and Liu et al. (2009). They found that the barrier layer exists in the subpolar region as well as the tropics and subtropical regions.

Long-term changes in the global distribution of near-surface salinity have been studied recently in detail under the Argo Program (e.g., Hosoda et al. 2009; Roemmich and Gilson 2009; Durack and Wijffels 2010). In areas of high near-surface salinity, salinity increased over the past 30–50 years, while it decreased in areas of low near-surface salinity, indicating that the global hydrological cycle has intensified during this period. This intensification is expected to continue into the future (e.g., Durack et al. 2012; Terray et al. 2012). These results also suggest that near-surface salinity changes have significant impacts on ocean stratification (e.g., Durack and Wijffels 2010).

Detailed examinations of long-term changes in salinity structure have been conducted in areas where long-term ocean monitoring is underway. For example, Crawford et al. (2007) investigated the profiles of temperature and salinity over 50 years along Line P between the North American west coast and central Gulf of Alaska. They found that salinity changes are dominated by variability in the halocline between 100- and 150-m depth and are attributable to changes in wind through surface Ekman transport and Ekman pumping. Oka et al. (2017) analyzed the 137°E repeat hydrographic section over 50 winters during 1967–2016 to examine interannual to interdecadal variation and long-term changes in salinity and temperature in the surface and intermediate layers of the western North Pacific, with a particular focus on freshening of the subtropical gyre. They found that rapid freshening along both isobars and isopycnals began in the mid-1990s and

Ryo Dobashi's current affiliation: Department of Oceanography, University of Hawai'i at Mānoa, Honolulu, Hawaii.

Corresponding author: Hiromichi Ueno, ueno@fish.hokudai.ac.jp

DOI: 10.1175/JPO-D-21-0056.1

continued over the last 20 years in the main upper thermocline and halocline layers of the western subtropical gyre.

Recently, the spatial distribution and seasonality of halocline structures in the subarctic North Pacific were investigated using Argo profiling float data in combination with surface flux data collected in 2003–17 (Katsura et al. 2020). This is the first study to target the halocline specifically. The mean distributions of permanent halocline depth and intensity corresponded to the winter mixed layer depth and sea surface salinity, respectively, indicating that the halocline forms in association with the development of the winter mixed layer. The summer seasonal halocline showed distinct zonal differences in frequency and intensity. Geostrophic and Ekman advection play important roles in driving the spatial differences in seasonal halocline intensity and depth.

Although the halocline plays an important role in biological production throughout the world oceans (Menviel et al. 2012), its spatiotemporal variation has not yet been clarified. In this study, we analyzed hydrographic data to clarify the distribution and interannual variation in haloclines in the World Ocean. We investigated winter haloclines to focus on the permanent halocline just below the winter mixed layer, which affects the timing and scale of the spring bloom. To use the uniform analysis method in the global ocean, we focused on the winter halocline even in the tropics (latitudes $< 20°$), where seasonality is less clear. Therefore, we performed additional analyses for the other seasons in the tropics to confirm that the results for the winter halocline were applicable to the other seasons in the tropics (appendix). We also concentrated on haloclines formed in the upper (shallower than 300 m) layer, corresponding to the climatological pycnocline depth, which is generally less than 300 m (Fiedler and Talley 2006). Although haloclines in which salinity (and temperature) strongly decrease with depth were sometimes observed, we focused on haloclines in which salinity increases with depth in this study.

2. Data and methods

Individual salinity and temperature profiles from the World Ocean Database 2013 (WOD13; Boyer et al. 2013), which includes extensive historical hydrographic data, were used for analyses of the halocline. We used profiling float (PFL) and high-resolution conductivity–temperature–depth (CTD) data at the observed depths in winter (December–March in the Northern Hemisphere and June–September in the Southern Hemisphere) from 2000 to 2017. In analyses of interannual variation, we regarded the winter of a year as the period from December of the preceding year to March of that year in the Northern Hemisphere (e.g., winter 2010 corresponds to the period from December 2009 to March 2010).

The main source of PFL data in WOD13 is the Argo project. We converted WOD13 PFL and CTD salinity and temperature data from the original depth profiles into 10-m intervals, as detailed below. We conducted this procedure because we evaluated the vertical gradient of salinity to define the halocline, as described below, and a generally uniform vertical salinity resolution was required to avoid artificial spatiotemporal variation in the halocline estimates. For each

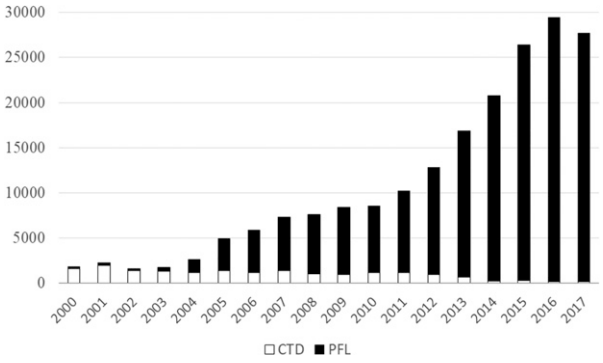

FIG. 1. Annual numbers of profiles used for the evaluation of halocline properties from 2000 to 2017 throughout the World Ocean.

10-m interval profile, we evaluated halocline strength and depth; then those values were averaged within each $4° \times 4°$ box across the World Ocean to visualize the distribution of the halocline.

The 10-m interval profiles were prepared as follows. First, we selected the shallowest-level data as the data point located closest to 10 m in depth among data collected at 8–22 m. We neglected profiles with no data between depths of 8 and 22 m. The shallowest-level salinity and temperature were considered the sea surface salinity and temperature, respectively. Then we identified the second shallowest-level data point as that located closest to the shallowest-level depth plus 10 m. If no observation was available in the depth range of the shallowest-level depth plus 5–20 m, the profile was neglected. The third shallowest-level data point was identified in the same manner as the second shallowest-level data point, and this process was repeated until we reached the depth of 295–315 m. When two data points are equally distant from the target depth, we used the deeper data. In this way, we obtained ~10-m interval profiles with ~30 levels between 8 and 315 m depth. We finally linearly interpolated these profiles to 10-m interval standard depth data with 30 levels from 10- to 300-m depth. In addition, we discarded profiles with downward salinity decrease greater than 0.2 per 10 m because such profiles possibly included strong downward salinity increase due to horizontal intrusion of fresher and cooler (density compensated) water masses as in Katsura et al. (2020), which was not the target of this study. Most of the profiles used for the evaluation of halocline properties were developed from PFL data, but CTD data were dominant from 2000 to 2003 (Fig. 1), a total of 196 816 profiles (CTD: 178 71, PFL: 178 945).

Using the 10-m interval profiles described above, we evaluated the properties of the halocline. First, we calculated the vertical salinity gradient ($\Delta S/\Delta$dep) for each layer between a level and the next (lower) level, where ΔS is the salinity increment between levels and Δdep is the vertical distance between the two levels (10 m). In this study, the halocline was defined as the layer of each profile with maximum $\Delta S/\Delta$dep (thick line segment in Fig. 2) below the surface mixed layer, while halocline strength (m^{-1}) and halocline depth (m) were defined as the maximum $\Delta S/\Delta$dep and the depth of the middle of the

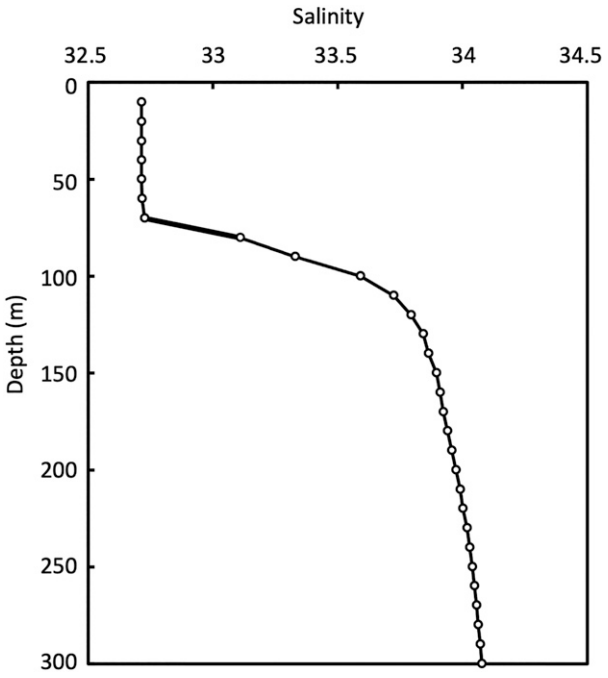

FIG. 2. An example of salinity profile obtained on 3 Feb 2017, at 53.506°N and 160.198°W. Thick solid segment indicates the location of the halocline.

layer, respectively. The sea surface salinity (SSS) and sea surface density are defined as salinity and density at 10-m depth, respectively. The surface mixed layer was considered the layer where the density was less than the sea surface density plus 0.03 kg m^{-3} (Oka et al. 2007).

Using the data for halocline strength and depth as well as SSS and mixed layer depth calculated from each profile, we evaluated their horizontal distributions averaged within each 4° × 4° box containing at least 10 profiles over the analysis period. The standard deviation of the values in each 4° × 4° box was also evaluated. To evaluate interannual variation of area A–I (Figs. 5 and 6), we evaluated annual-mean (i.e., winter mean) values with standard errors for the years with ≧10 profiles in each area. In addition, we considered grids where the average halocline strength was weaker than 1.0×10^{-2} m^{-1} as having no halocline, as it is not appropriate to regard a weak salinity gradient layer as a halocline. The threshold of 1.0×10^{-2} m^{-1} was used, in accordance with Katsura et al. (2020).

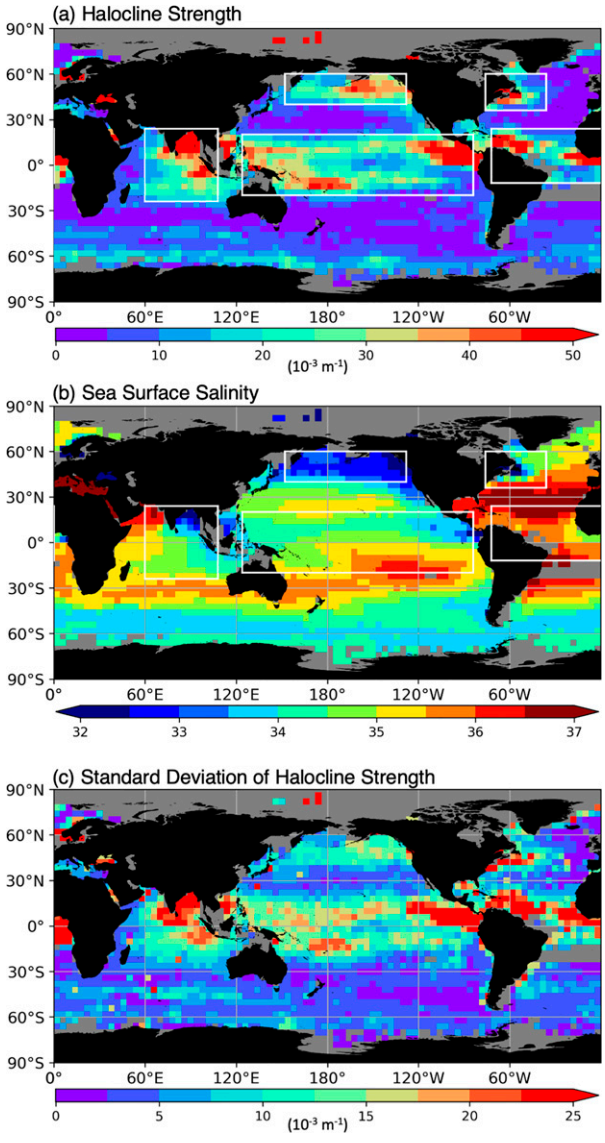

FIG. 3. Climatological winter distributions of (a) halocline strength (10^{-3} m^{-1}), (b) sea surface (10-m depth) salinity, and (c) standard deviation of halocline strength (10^{-3} m^{-1}). Gray boxes indicate areas where the number of profiles was less than 10. Five rectangles outlined in white represent the areas used for correlation analyses in section 3 (northern North Pacific: 40°–60°N, 152°E–128°W; equatorial Pacific: 20°S–20°N, 124°E–84°W; northwestern North Atlantic: 36°–60°N, 36°–76°W; equatorial Atlantic: 12°S–24°N, 0°–72°W; and Indian Ocean: 24°S–24°N, 60°–108°E).

3. Halocline distribution in the World Ocean

As determined from wintertime hydrographic data, a halocline was generally observed at latitudes between 20°S and 20°N, in the northern North Pacific, and in the Southern Ocean (Fig. 3a). It was absent, that is halocline strength was weaker than 1.0×10^{-2} m^{-1}, in the central subtropical regions (Fig. 3a). The halocline was mostly distributed at depths shallower than 100 m in the area between 20°S and 20°N and at depths of 100–200 m in the northern North Pacific and the Southern Ocean around or south of 60°S (Fig. 4a). The standard deviation of the halocline strength and depth evaluated in each 4° × 4° box was relatively large in the area where halocline strength and depth are relatively strong and deep, respectively (Figs. 3c and 4c).

In the Pacific Ocean, a strong halocline (>50×10^{-3} m^{-1}) was observed in the far eastern tropical Pacific at depths shallower than 50 m (Figs. 3a and 4a). In this area, sea surface

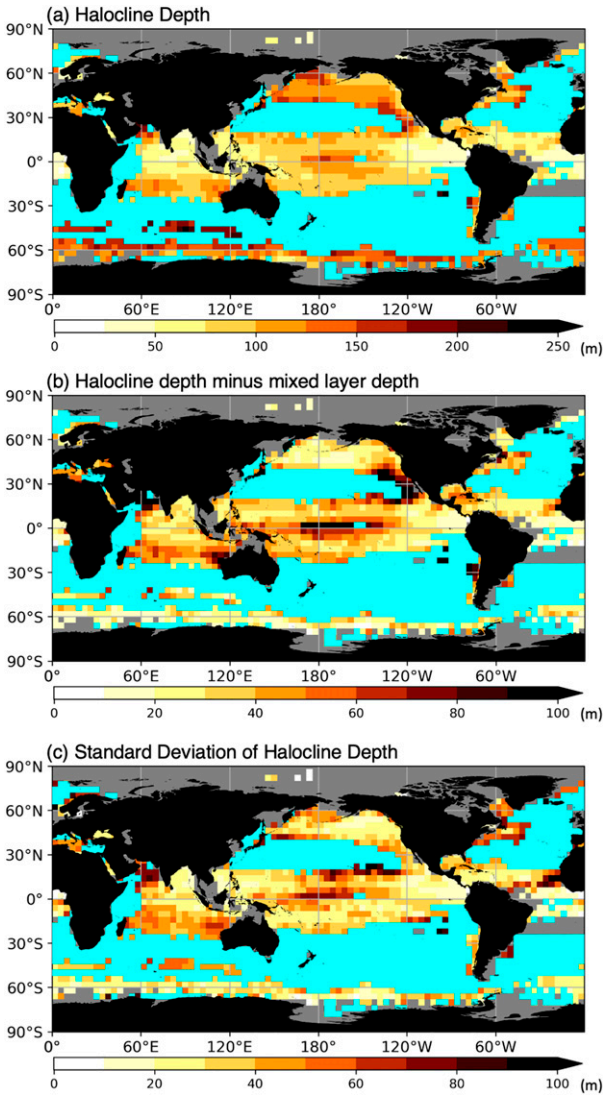

FIG. 4. Climatological winter (a) halocline depth (m) and (b) difference between halocline depth and mixed layer depth (halocline depth minus mixed layer depth) (m) and (c) standard deviation of halocline depth (m). Gray and light blue grids contain profiles fewer than 10 and have no halocline (i.e., halocline strength $< 10^{-2}$ m^{-1}), respectively.

salinity (SSS) was low (Fig. 3b) due to high summer monsoon rainfall along the Pacific slope of Central America (Amador et al. 2006; Fiedler and Talley 2006), suggesting that enhanced surface freshwater flux formed a strong halocline by lowering surface salinity. A relatively strong halocline ($>30 \times 10^{-3}$ m^{-1}) was observed in the far western tropical Pacific and along the latitudes of 10°N and 10°S at depths between 50 and 100 m, while the halocline was relatively weak along the equator between 120°W and 180°. Halocline formation was also observed over the subarctic North Pacific and along the west coast of the United States and Mexico. In these regions, the halocline depth was generally greater than 100 m.

In the Atlantic Ocean, the halocline area was relatively small; a strong halocline was observed near the eastern and western coasts in the tropics and along the east coast of the United States and Canada (Fig. 3a). The strong halocline near the eastern and western coasts in the tropics corresponds to the area of relatively low SSS (Fig. 3b). In these areas, strong rainfall, high-level discharge from the Congo and Amazon Rivers, and surface advection create a low SSS (e.g., Foltz and McPhaden 2008; Mignot et al. 2012; Da-Allada et al. 2013), possibly explaining the strong halocline. In the Indian Ocean, the halocline was strongest in the Bay of Bengal (strength $> 50 \times 10^{-3}$ m^{-1}). In this region, strong rainfall and runoff produced a fresh surface layer (e.g., Shetye et al. 1996; Agarwal et al. 2012), probably enhancing the halocline. The halocline generally weakened toward the west and did not exist or was very weak near the western edge of the Indian Ocean, unlike in the Pacific and Atlantic Oceans. In the Southern Ocean, a weak halocline ($10–20 \times 10^{-3}$ m^{-1}) was observed around 60°S.

The halocline is expected to be strong in areas where the salinity above the halocline is low and/or the salinity below the halocline is high. Generally, horizontal variation in shallower-layer salinity, that is the salinity above the halocline, is greater than that in the deeper layer. Thus, the horizontal distribution of the halocline is expected to be generally determined by the shallower-layer salinity distribution, as discussed above. Therefore, here, we compare the horizontal distribution of the halocline and the SSS, a surrogate for shallower-layer salinity, which is associated with the global water cycle (e.g., Hosoda et al. 2009; Yu 2011). The strong halocline tended to be distributed in areas where SSS was low, e.g., the far eastern tropical Pacific, the subarctic North Pacific, and the Bay of Bengal (Figs. 3a,b). Next, we determined the correlation coefficients between halocline strength and the SSS for the five areas outlined in Figs. 3a and 3b, excluding the grids with halocline strength weaker than 10×10^{-3} m^{-1}. The correlation coefficients for the northern North Pacific, the equatorial Pacific, the northwestern North Atlantic, the equatorial Atlantic, and the Indian Ocean were −0.64, −0.63, −0.87, −0.58, and −0.93, respectively, all of which were significant at the 99% confidence level. These results suggest that the horizontal halocline distribution was mostly determined by the SSS, and that SSS could be used as a proxy for halocline strength.

The area with no halocline (i.e., the area where halocline strength was weaker than 1.0×10^{-2} m^{-1} in Fig. 3a) generally corresponds to the area of maximum SSS, e.g., the area of SSS > 35 in the North Pacific (Fig. 3b). These SSS maxima mostly occur in the trade wind and subtropical high-pressure regions, where annual evaporation exceeds precipitation (e.g., Talley et al. 2011), which likely prevents halocline formation. Figure 4b shows the difference between the depths of the halocline and the mixed layer. In strong halocline regions, such as the eastern edge of the tropical Pacific, the western part of the Gulf of Alaska, and the Bay of Bengal, this difference was relatively small, indicating that the halocline was located just below the mixed layer in winter. In the area off the west coast of United States and Mexico between 20° and 40°N, the difference was relatively large, in part because salinity in this area

is strongly affected by low-salinity water subduction to the subsurface layer from the northern region, forming halocline in the deep layer relative to winter mixed layer bottom (e.g., Talley 1985). In this region, the standard deviation of the halocline depth was relatively small compared with deep halocline depth.

4. Interannual variability in the halocline

Halocline strength showed interannual variability, which differed among areas e.g., in magnitude and mechanism as follows (Fig. 5, Table 1). Areas were selected where the halocline was relatively strong and more than 9 profiles were available per winter for most of the analysis period. In the tropical region (areas A–E), halocline strength varied interannually, with a standard deviation $> 5.0 \times 10^{-3}$ m^{-1}. Halocline strength tended to be high when SSS was low; the correlation coefficient between halocline strength and SSS was less than −0.65 and was significant at the 99% confidence level. These results suggest that the interannual variation in halocline strength in the tropical region is determined primarily by SSS variation. We further investigated the relation between the interannual variation of halocline strength in areas A–E and Southern Oscillation index (SOI: https://www.ncdc.noaa.gov/teleconnections/enso/indicators/soi/). As the result, we found that the SOI was negatively correlated to the halocline strength in area B (correlation coefficient: −0.79). This is consistent with ENSO-related precipitation pattern, that is, strong precipitation in area B during El Niño event (e.g., Wallace et al. 1998), suggesting that the movement of precipitation area affects the interannual variation of halocline strength in the central tropical Pacific. Along the eastern edge of the tropical Pacific (area C), SSS and halocline strength appear to decrease and increase, respectively, during our analysis period. This SSS trend (−0.4 during 2002–17) is consistent with the findings of Hosoda et al. (2009) and Durack and Wijffels (2010) qualitatively, although the magnitude of the trend is stronger than theirs probably because our analysis period is differed from theirs (1960–2007 and 1950–2008, respectively).

In the northwestern North Pacific (area F), the interannual variability of halocline strength and its relationship with SSS was weaker than in the tropics, although the correlation coefficient was also negative (Fig. 5 and Table 1). By contrast, in the Gulf of Alaska (area G), the correlation coefficient was 0.47, indicating that halocline tended to be strong when SSS was high (significant at the 95% confidence level). In the northwestern North Atlantic (area H), halocline strength also varied synchronously with SSS (correlation coefficient: −0.71). The Southern Ocean (area I) had the weakest interannual variation in the halocline, which showed no correlation with SSS (Fig. 5 and Table 1).

Figure 7a shows the distribution of correlation coefficients between the interannual variation in halocline strength and SSS. The correlation coefficient was negative (halocline was strong when SSS was low) in most regions. This result suggests that the interannual variation in the halocline was determined primarily by variation in SSS throughout the World Ocean. In the Gulf of Alaska, on the other hand, the correlation coefficient was positive, suggesting that another mechanism was dominant in this area. This region is discussed in the next section. Figure 7c shows the distribution of correlation coefficients between the interannual variation in SSS and mixed layer depth. This figure indicates that in many regions SSS was high in the year of deep mixed layer, suggesting that deep mixed layer increased SSS through entrainment of saline subsurface water. In contrast, the correlation coefficient was mostly negative in the far eastern tropical Pacific, where the halocline strength was very strong due to strong precipitation and thus low SSS (Fiedler and Talley 2006).

Halocline depth also varied interannually (Fig. 6), with standard deviations from 5.1 m in area C to 20.1 m in area B; both areas are located in the tropical Pacific (Table 2). Figure 6 and Table 2 also show that spatial variation of halocline depth is larger than interannual variation in the tropics (areas A–E) in contrast to high latitudes (areas F–I) with weak spatial variation. The halocline was located just below the mixed layer in many areas in the World Ocean (Fig. 4b); we investigated the relationship between the interannual variation in halocline depth and mixed layer depth (Table 2). The correlation coefficients were generally positive and significant, particularly at high latitudes (areas F–I, Table 2 and Fig. 7b). This result is consistent with those of Fiedler and Talley (2006), who found that the pycnocline is governed primarily by salinity stratification at high latitudes. Figure 7b also indicates that the area of weak correlation (e.g., off the west coast of United states and around 0°–8°N in the central Pacific) mostly corresponds to the area with large depth difference between the halocline depth and mixed layer depth (Fig. 4b), suggesting that the halocline located enough deeper than the mixed layer bottom tends to be less influenced by the mixed layer depth. In addition, the seasonality is less clear in the tropics, which might affect the relation between the mixed layer depth and the halocline depth especially in the central tropical Pacific as discussed in appendix.

5. Interannual variability of the halocline in the Gulf of Alaska

Halocline strength tended to be strong when SSS was high in the Gulf of Alaska, as described in the previous section. In this section, we explore the mechanism driving this tendency. Figure 8a shows average salinity profiles for the Gulf of Alaska (area G) in the strongest halocline winters (red, pink, and yellow colors) and the weakest halocline winters (black, blue, and light blue colors). In strong halocline years, the salinities of the subsurface layer and the mixed layer were mostly higher than in weak halocline years. In addition, the isopycnal of 26.5σ_θ was located at a shallower depth (149-m depth on average) in strong halocline years relative to weak halocline years (164-m depth). These results suggest that high-salinity subsurface layers were uplifted in strong halocline years.

In the Gulf of Alaska, cyclonic circulation forms due to the input of positive wind stress curl, Ekman divergence and the associated Ekman upwelling. Therefore, we examined the interannual variation in wind stress curl averaged over area G. We found that it was well correlated with halocline strength

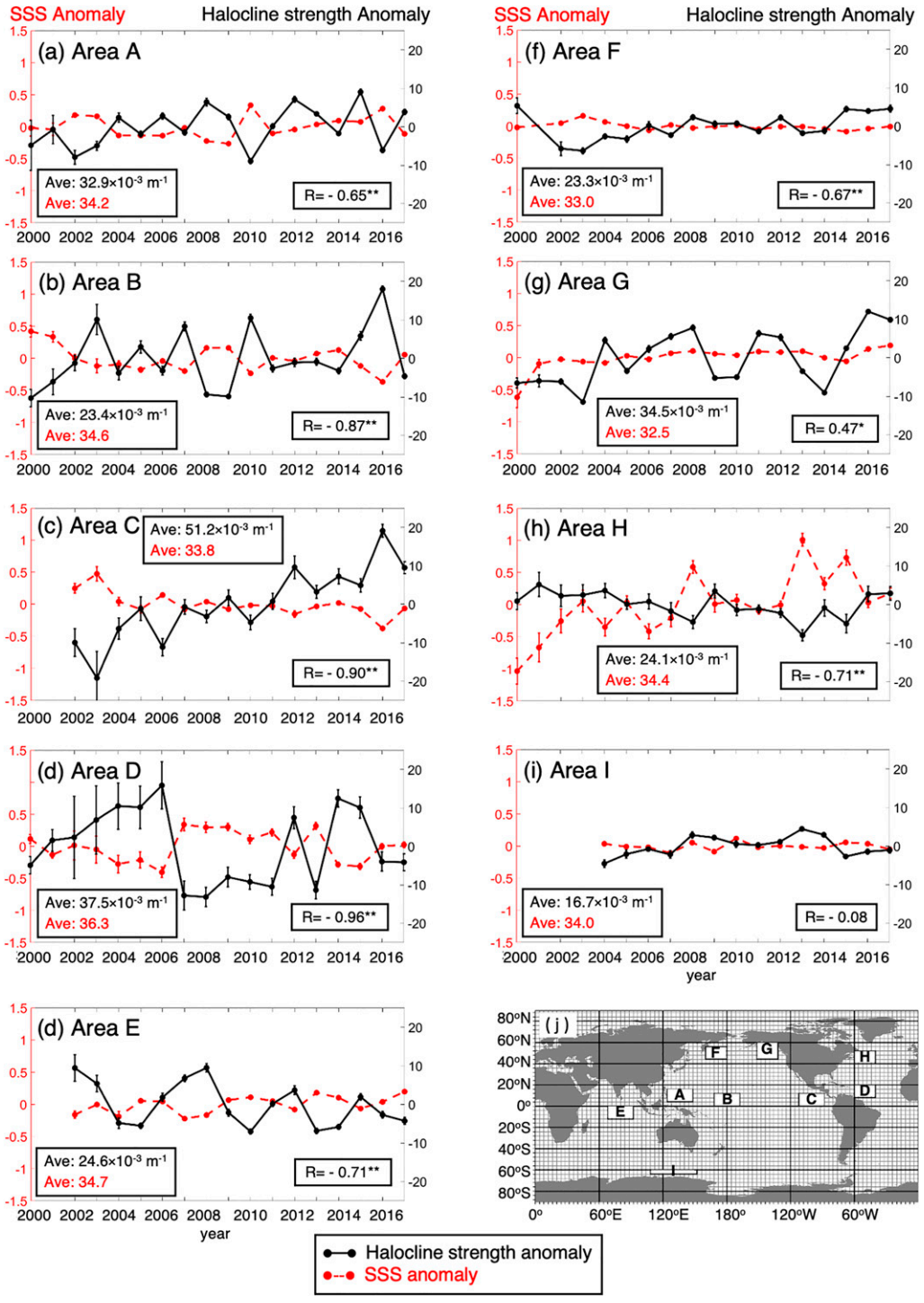

FIG. 5. Interannual variation in halocline strength anomaly (solid black line with dots; right axis; 10^{-3} m^{-1}) and sea surface salinity (SSS) anomaly (dashed red line with dots; left axis) in winter averaged across (a) area A (4°–16°N, 124°–148°E), (b) area B (0°–12°N, 168°E–168°W), (c) area C (0°–12°N, 88°–112°W), (d) area D (8°–20°N, 40°–60°W), (e) area E (0°–12°S, 68°–92°E), (f) area F (44°–56°N, 160°–180°E), (g) area G (44°–60°N, 132°–152°W), (h) area H (40°–52°N, 40°–60°W), and (i) area I (60°–64°S, 108°–152°E) with standard errors (bars). Dots were plotted when more than 9 profiles existed in the area and in the year (winter). The *R* in (a)–(i) indicates the correlation coefficient between halocline strength anomaly and SSS anomaly (** and *: significant at the 99% and 95% confidence level, respectively), and Ave in black (red), which are used for anomaly calculation, represents halocline strength (SSS) averaged for the analysis period using values averaged in each year. (j) The areas for (a)–(i).

TABLE 1. Average, maximum, minimum, and standard deviation of interannual variation in winter halocline strength ($\times 10^{-3}$ m^{-1}) and correlation coefficient between winter halocline strength and winter SSS for areas A–I (** = significant at the 99% confidence level, * = significant at the 95% confidence level).

Area	Average	Maximum	Minimum	Standard deviation	Correlation coefficient
A	32.9	42.0	24.0	5.19	−0.65**
B	23.4	41.5	13.2	7.83	−0.87**
C	51.2	70.3	32.0	9.32	−0.90**
D	37.5	53.4	24.3	9.75	−0.96**
E	24.5	34.1	17.5	5.71	−0.72**
F	23.3	28.6	16.9	3.55	−0.67**
G	34.5	46.5	23.1	7.03	0.47*
H	24.0	29.2	16.0	3.44	−0.71**
I	16.7	21.1	12.2	2.53	−0.08

(correlation coefficient: 0.48, significant at the 95% confidence level). This suggests that strong wind stress curl increases Ekman upwelling, pushes high-salinity water up into the subsurface layer, and strengthens the halocline. Through the same mechanism, strong wind stress curl may result in high SSS. This process may explain why the halocline tends to be strong when SSS is high in the Gulf of Alaska. Crawford et al. (2007) found that salinity changes in the halocline between 100- and 150-m depth in the Gulf of Alaska are attributable to changes in wind through surface Ekman transport and Ekman pumping, consistent with our suggestion that the wind stress curl affects the halocline although their analysis period was 1956–2005.

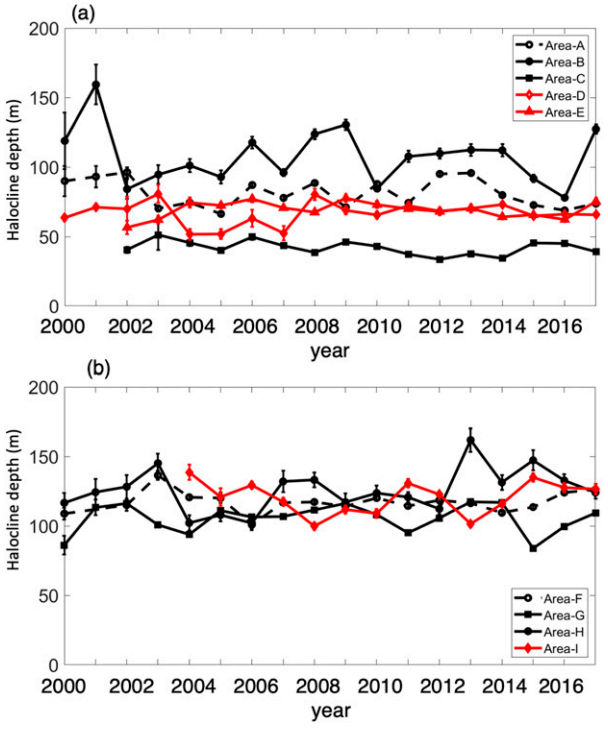

FIG. 6. Interannual variation in winter halocline depth (m) averaged across (a) areas A–E and (b) areas F–I, with standard errors (bars). The areas are shown in Fig. 5j.

Wind stress curl was not correlated with SSS (correlation coefficient: 0.13), likely because precipitation also plays an important role in driving the interannual variation in SSS. In addition, mixed layer depth was strongly correlated to SSS (correlation coefficient: 0.86 significant at the 99% confidence level), suggesting that deep mixed layer increased SSS through entrainment of saline subsurface water in this region. The relation between the halocline strength and Pacific decadal oscillation (PDO) index (https://www.ncdc.noaa.gov/teleconnections/pdo/), North Pacific Gyre Oscillation index (NPGO) index (http://www.o3d.org/npgo/), and SOI was weak (absolute values of correlation coefficient ≦ 0.43).

6. Summary and discussion

We investigated the distribution and interannual variation in the winter halocline in the upper layers of the World Ocean through analyses of hydrographic data from the World Ocean Database 2013 using a simple definition of the halocline. A halocline was observed in the tropics, equatorward portions of subtropical regions, the subarctic North Pacific, and Southern Ocean, but was absent where halocline strength was weaker than 1.0×10^{-2} m^{-1}, particularly in the central subtropics. A strong halocline tended to be observed in areas where SSS was low. The interannual variation in halocline strength was correlated with variation in SSS. The correlation coefficients were usually negative: the halocline was strong when SSS was low. However, in the Gulf of Alaska in the northeastern North Pacific, the correlation coefficient was positive.

In the Gulf of Alaska, we propose that halocline strength is influenced by interannual variation in Ekman pumping. Here, we briefly discuss the relationship between halocline strength and Ekman pumping semiquantitatively. Considering the one-dimensional advective–diffusive balance:

$$w\frac{\partial S}{\partial z} = K_z\frac{\partial^2 S}{\partial z^2}, \tag{1}$$

where w and K_z are the vertical (entrainment) velocity and diffusivity, respectively, salinity (S) within the halocline is represented as

$$S = S_\infty + (S_0 - S_\infty)e^{(z-z_s)/\delta_s}, \tag{2}$$

TABLE 2. Average, maximum, minimum, and standard deviation of interannual variation in winter halocline depth (m) and correlation coefficient between winter halocline depth and winter mixed layer depth for areas A–I (** = significant at the 99% confidence level, * = significant at the 95% confidence level).

Area	Average	Maximum	Minimum	Standard deviation	Correlation coefficient
A	81.3	96.3	66.4	10.3	0.74**
B	107.9	159.3	78.0	20.1	0.07
C	41.9	51.3	33.6	5.15	0.68**
D	66.7	80.7	51.7	8.34	0.85**
E	69.2	77.7	56.6	5.91	0.60*
F	117.2	136.4	100.9	7.76	0.91**
G	105.4	117.4	83.7	10.3	0.58*
H	125.7	161.8	102.0	15.6	0.84**
I	120.5	138.6	100.0	11.9	0.83**

assuming that w and K_z are constant and that the thickness of the halocline (δ_S) is represented as w/K_z (Vallis 2006). The terms S_∞ and S_0 are salinity of the deep layer below the halocline and of the surface mixed layer, respectively, and z_s is the surface mixed layer depth. Therefore, the halocline strength ($\tilde{S}$) just below the surface mixed layer is represented as

$$\tilde{S} = -\left(\frac{\partial S}{\partial z}\right)_{z=z_s} = \frac{S_\infty - S_0}{\delta_s} = \frac{S_\infty - S_0}{K_z} w_E, \tag{3}$$

where w_E is Ekman pumping velocity [$=\mathrm{curl}\tau/(\rho_0 f_0)$], and ρ_0 and f_0 are density and the Coriolis parameter, respectively, which are set to $\sim 10^3$ kg m^{-3} and 10^{-4} s^{-1}. Assuming that K_z is 10^{-4} m^2 s^{-1} (e.g., Waterhouse et al. 2014), $(S_\infty - S_0)$ is 1.2 (Fig. 8a), and the fluctuation range of curlτ is 5–10 $\times$ 10^{-8} N m^{-3} (Fig. 8b), the range of $\tilde{S}$ fluctuations is estimated to be 6–12 $\times$ 10^{-3} m^{-1}, which is of the same order as the fluctuation range of halocline strength obtained from hydrographic data, 10–20 $\times$ 10^{-3} m^{-1} (Fig. 8b). This result quantitatively supports our hypothesis that strong wind stress curl strengthens the halocline through increased Ekman upwelling.

The horizontal distribution of long Rossby wave speed (e.g., Fig. 16 in Killworth et al. 1997) also supports the hypothesis in the Gulf of Alaska delineated by (1). Considering a quasigeostrophic potential vorticity equation in a rigid-lid two-layer ocean as in Mitsudera et al. (2018), the evolution equation for the upper layer (the layer above the halocline) thickness h is generally expressed as follows:

$$\frac{\partial h}{\partial t} + C_x \frac{\partial h}{\partial x} = -w_E, \tag{4}$$

where t and x are time and zonal position, respectively, and C_x denotes the baroclinic Rossby wave speed in the presence of ambient baroclinic and barotropic flow. In the tropics and subtropics (<35°), $|C_x|$ = is larger than ~3 cm s^{-1} (Fig. 16 in Killworth et al. 1997), suggesting that $C_x \partial h/\partial x$ term plays an important role in the h variation. In the Kuroshio Extension region, for example, Qiu (2003) indicated that the decadal variation of Kuroshio Extension jet is related to the baroclinic Rossby wave propagated from the east. In the Gulf of Alaska, on the other hand, C_x is close to zero (Fig. 16 in Killworth et al. 1997), suggesting

$$\frac{\partial h}{\partial t} = -w_E. \tag{5}$$

Equation (5) indicates that h responds to local w_E, that is, the halocline is lifted locally by the Ekman pumping until it becomes thin enough to be steady (in terms of a seasonal time scale) below the mixed layer base. In the steady state, w_E is balanced with the entrainment velocity w in (1), and hence the advective–diffusive balance (1) is achieved as for the salinity budget. Therefore, in the steady state, (5) with the entrainment term is consistent with (3), assuming that

$$\text{entrainment} \rightarrow \frac{K_z}{\delta_s} \text{ in the steady state.} \tag{6}$$

The discussions above suggest that halocline strength, or halocline thickness δ_s, is influenced by interannual variation in Ekman pumping in the Gulf Alaska, where baroclinic Rossby wave speed in the presence of ambient baroclinic and barotropic flow is close to zero as well as strong halocline is observed.

The lag-correlation coefficients between the halocline strength and wind stress curl averaged over area G (0.39, 0.19, −0.04, and 0.41 for 3-, 6-, 9- and 12-months lag, respectively) are smaller than that without lag (0.48), consistent with the hypothesis discussed above. However, more detailed investigation with e.g., numerical experiment is necessary to understand the mechanism determining the interannual variation of halocline strength in the Gulf of Alaska.

The distribution of the halocline was similar to that of the barrier layer, i.e., the layer between the halocline (salinity stratification) in the surface isothermal layer and the thermocline located below (de Boyer Montégut et al. 2007; Liu et al. 2009). Regions lacking the halocline (the light blue regions in Fig. 4) mostly corresponded to regions without barrier layers (e.g., Fig. 2 in Liu et al. 2009). This is because, by definition, barrier layers cannot exist in the absence of salinity stratification sufficiently strong to

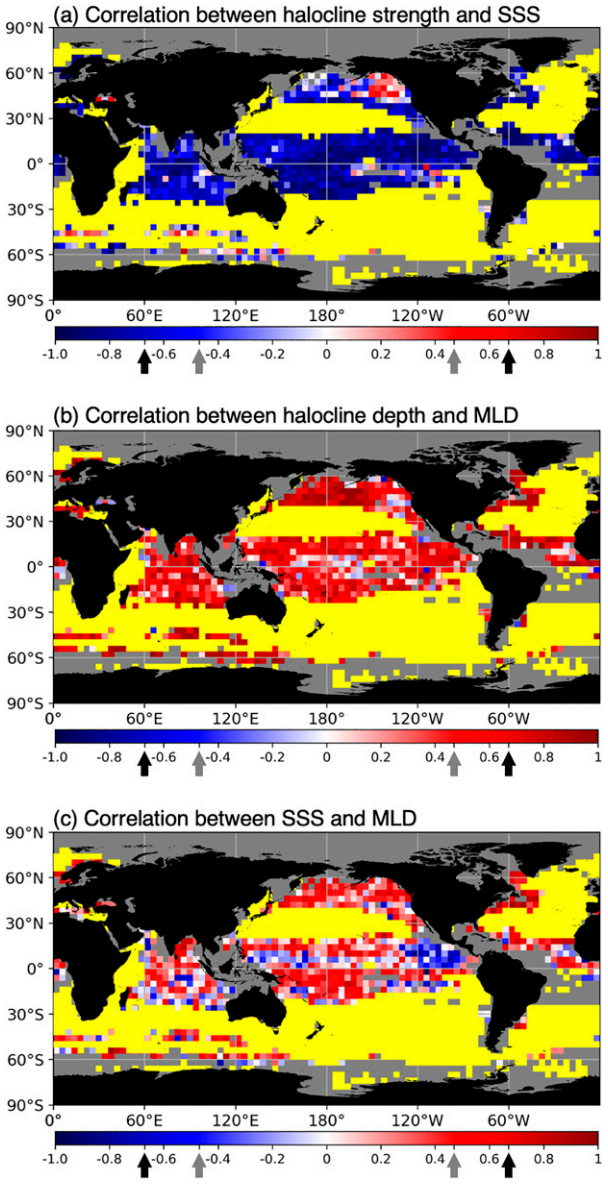

FIG. 7. Correlation coefficients between the interannual variation in (a) winter halocline strength (m^{-1}) and winter SSS, (b) winter halocline depth (m) and winter mixed layer depth (MLD; m) and (c) SSS and MLD (m). Correlation coefficients were evaluated for the boxes with more than eight annual (i.e., winter) averages (each annual average was evaluated when more than two profiles existed in a box and in a year) during 2000–17. Gray and yellow boxes indicate those with data less than 9 years and those without halocline (i.e., halocline strength $< 10^{-2}$ m^{-1}, see Fig. 3a), respectively. Black and gray arrows indicate the correlation coefficients significant at the 95% confidence level for boxes with 9 annual averages and 18 annual averages, respectively.

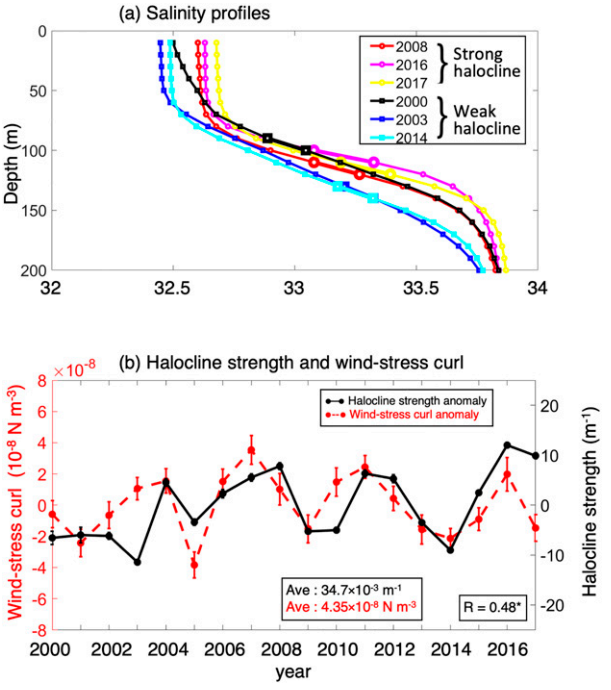

FIG. 8. (a) Salinity profiles averaged across the Gulf of Alaska (area G: 44°–60°N, 132°–152°W) in the strongest halocline winters (red, pink, and yellow colors) and the weakest halocline winters (black, blue, and light blue colors) and (b) interannual variation in wind stress curl anomaly and halocline strength anomaly in winter averaged across area G, with standard errors (bars). The thick segments in (a) correspond to the layer with the strongest salinity gradient in the averaged profile, in contrast to the halocline strength and depth in Figs. 5 and 6, which were evaluated as the average of halocline strength and depth for each profile in each winter and area. In (a), profiles with very low surface salinity less than 32, affected by freshwater from the coast (e.g., Crawford et al. 2007), were not used for the averaging procedure to avoid artificial unrealistic averaged profiles. In (b), the plots for the halocline strength anomaly are the same as in Fig. 5g. The R in (b) indicates the correlation coefficient between halocline strength anomaly and wind stress curl anomaly (* significant at the 95% confidence level), and Ave in red, which are used to calculate wind stress curl anomaly, represents 18-yr averaged wind stress curl using values averaged in each year. The wind stress was evaluated from NCEP–NCAR reanalysis 10-m wind data (Kalnay et al. 1996): wind stress $= C_D\rho_A|U_{10}|U_{10}$, where C_D is the drag coefficient (1.2×10^{-3}), ρ_A is the density of air at sea level (1.178 kg m^{-3}), and U_{10} is wind velocity at 10 m above the sea surface.

form the bottom of the mixed layer. However, the halocline was not always located in the isothermal layer, which caused marked differences between the distributions of the halocline and barrier layer in some areas. For example, in the far eastern tropical Pacific, a significant barrier layer was not observed although a strong halocline was present. This is because the halocline and thermocline coexist in the same layer in this region (e.g., Fiedler and Talley 2006; Helber et al. 2012), indicating that the halocline defined in the present study captured a different ocean structure than the barrier layer. Such a difference also occurred in the eastern equatorial Atlantic, where a significant barrier layer was not observed but a strong halocline existed.

The winter halocline in the present study mostly corresponds to the permanent halocline in the subarctic North Pacific (Katsura et al. 2020) and salinity difference between the surface mixed layer bottom and surface isothermal layer bottom (ΔS: negative values correspond to salinity increase with depth, Liu et al. 2009). Katsura et al. (2020) defined a vertical salinity gradient maximum below 70 dbar as a permanent halocline thorough analysis of profiles in all seasons considering seasonal halocline as well as permanent halocline. Their climatological depth and strength of permanent halocline in the subarctic North Pacific (Fig. 4 in Katsura et al. 2020) shows that the permanent halocline is strong around 160°W and 50°N ($>4 \times 10^{-2}$ dbar^{-1}) and 165°E and 50°N ($>2 \times 10^{-2}$ dbar^{-1}), which correspond to Fig. 3a in the present study, suggesting that the winter halocline in the present study well detected the permanent halocline in the subarctic North Pacific. Liu et al. (2009) showed ΔS was large at latitudes between 20°S and 20°N, in the northern North Pacific in January–March, and in the Southern Ocean in July–August, well corresponding to the winter halocline distribution (Fig. 3a). However, Liu et al. (2009) showed weak ΔS in the far eastern tropical Pacific, where this study detected the strongest halocline. This is because the halocline and thermocline coexist in the same layer in this region as discussed in the previous paragraph.

Acknowledgments. The authors thank Takuya Nara and Yang Liu. The authors also thank two anonymous reviewers for their constructive and helpful comments. This work was supported by JSPS KAKENHI Grant number 18K03736.

APPENDIX

Seasonality of the Halocline in the Tropics

Since the present study focused on the winter halocline even in the tropics, where seasonality is less clear, we performed additional analyses for the other seasons in the tropics. Figs. A1 and A2 show halocline strength and depth in each season. Halocline strength shows strong seasonal variation in the tropics especially along ~10°N and ~10°S, which correspond to intertropical convergence zone (ITCZ) and South Pacific convergence zone (SPCZ), where strong seasonal variation in precipitation is observed. Halocline depth, in contrast, shows weak seasonal variation or is relatively deep in January–March/July–September especially in the far western or eastern tropical Pacific, in the tropical Atlantic and in the tropical Indian Ocean in the Northern/Southern Hemisphere, respectively, suggesting that in these regions winter halocline could correspond to permanent halocline, which is the target of the present study. However, in the central tropical Pacific, halocline depth was relatively deep in October–March and relatively shallow in April–September in the Southern Hemisphere, that is, summer halocline was deeper than winter halocline. In this region, winter halocline might not represent permanent halocline.

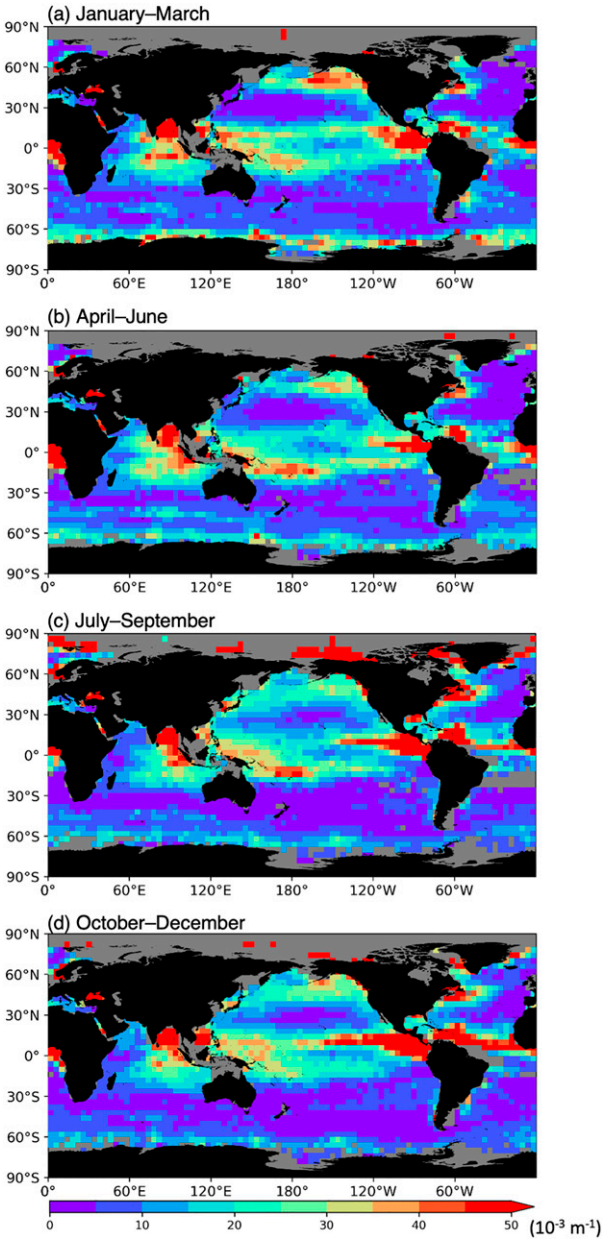

FIG. A1. Climatological distributions of halocline strength (10^{-3} m^{-1}) in (a) January–March, (b) April–June, (c) July–September and (d) October–December. Gray boxes indicate areas where the number of profiles was less than 10.

We evaluated the correlation coefficients between the horizontal distribution of halocline strength and SSS in January–March, April–June, July–September, and October–December for the equatorial Pacific, the equatorial Atlantic, and the Indian Ocean outlined in Figs. 3a and 3b. The correlations were all significant at the 99% confidence level, suggesting that the horizontal halocline distribution was mostly determined by the SSS throughout the year in the tropics. We also investigated the relation

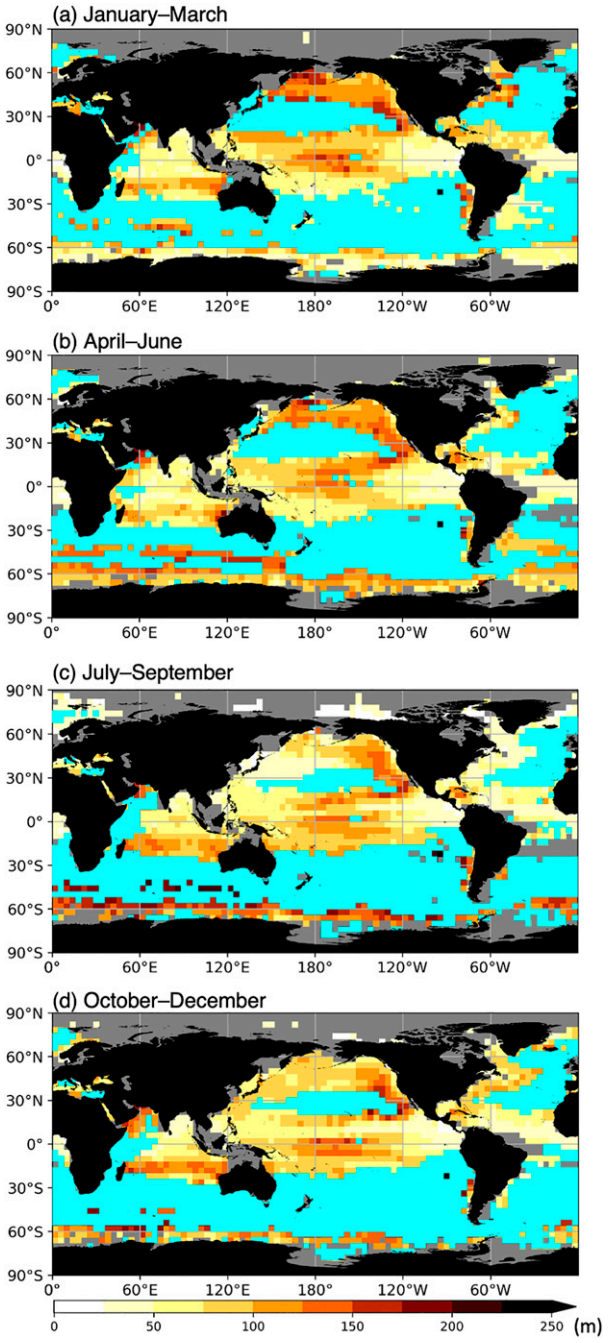

FIG. A2. As in Fig. A1, but for halocline depth (m). Gray and light blue grids contain profiles fewer than 10 and have no halocline (i.e., halocline strength $< 10^{-2}$ m^{-1}), respectively.

between the halocline strength and SSS in the interannual variation in areas A–E. In areas B–E, the interannual variation in halocline strength was determined primarily by SSS variation [significant at the 99% confidence level, except for area C in July–September (95% confidence level)]. In area A, on the other hand, correlation between halocline strength and SSS was weak in July–September and October–December (correlation coefficient: −0.23 and −0.23, respectively), suggesting that SSS was not a dominant factor controlling the interannual variation of halocline strength in this area and seasons. These results suggest that more detailed analyses are needed to understand the distribution and interannual variation of permanent halocline in the tropics.

REFERENCES

Agarwal, N., R. Sharma, A. Parekh, S. Basu, A. Sarkar, and V. K. Agarwal, 2012: Argo observations of barrier layer in the tropical Indian Ocean. *Adv. Space Res.*, **50**, 642–654, https://doi.org/10.1016/j.asr.2012.05.021.

Amador, J. A., E. J. Alfaro, O. G. Lizano, and V. O. Magana, 2006: Atmospheric forcing of the eastern tropical Pacific: A review. *Prog. Oceanogr.*, **69**, 101–142, https://doi.org/10.1016/j.pocean.2006.03.007.

Boyer, T. P., and Coauthors, 2013: World Ocean Database 2013. NOAA Atlas NESDIS 72, 209 pp., https://doi.org/10.7289/V5NZ85MT.

Crawford, W. R., J. Galbraith, and N. Bolingbroke, 2007: Line P ocean temperature and salinity 1956–2005. *Prog. Oceanogr.*, **75**, 161–178, https://doi.org/10.1016/j.pocean.2007.08.017.

Da-Allada, C. Y., G. Alory, Y. du Penhoat, E. Kestenare, F. Durand, and N. M. Hounkonnou, 2013: Seasonal mixed-layer salinity balance in the tropical Atlantic Ocean: Mean state and seasonal cycle. *J. Geophys. Res. Oceans*, **118**, 332–345, https://doi.org/10.1029/2012JC008357.

de Boyer Montégut, C., J. Mignot, A. Lazar, and S. Cravatte, 2007: Control of salinity on the mixed layer depth in the world ocean: 1. General description. *J. Geophys. Res.*, **112**, C06011, https://doi.org/10.1029/2006JC003953.

Durack, P. J., and S. E. Wijffels, 2010: 50-year trends in global ocean salinities and their relationship to broad-scale warming. *J. Climate*, **23**, 4342–4362, https://doi.org/10.1175/2010JCLI3377.1.

——, ——, and R. J. Matear, 2012: Ocean salinities reveal strong global water cycle intensification during 1950 to 2000. *Science*, **336**, 455–458, https://doi.org/10.1126/science.1212222.

Emile-Geay, J., M. A. Cane, N. Naik, R. Seager, A. C. Clement, and A. van Geen, 2003: Warren revisited: Atmospheric freshwater fluxes and "Why is no deep water formed in the North Pacific." *J. Geophys. Res.*, **108**, 3178, https://doi.org/10.1029/2001JC001058.

Fiedler, P. F., and L. D. Talley, 2006: Hydrography of the eastern tropical Pacific: A review. *Prog. Oceanogr.*, **69**, 143–180, https://doi.org/10.1016/j.pocean.2006.03.008.

Foltz, G. R., and M. J. McPhaden, 2008: Seasonal mixed layer salinity balance of the tropical North Atlantic Ocean. *J. Geophys. Res.*, **113**, C02013, https://doi.org/10.1029/2007JC004178.

Helber, R. W., A. B. Kara, J. G. Richman, M. R. Carnes, C. N. Barron, H. E. Hurlburt, and T. Boyer, 2012: Temperature versus salinity gradients below the ocean mixed layer. *J. Geophys. Res.*, **117**, C05006, https://doi.org/10.1029/2011JC007382.

Hosoda, S., T. Suga, N. Shikama, and K. Mizuno, 2009: Global surface layer salinity change detected by Argo and its implication for hydrological cycle intensification. *J. Oceanogr.*, **65**, 579–586, https://doi.org/10.1007/s10872-009-0049-1.

Kalnay, E., and Coauthors, 1996: The NCEP/NCAR 40-Year Reanalysis Project. *Bull. Amer. Meteor. Soc.*, **77**, 437–471, https://doi.org/10.1175/1520-0477(1996)077<0437:TNYRP>2.0.CO;2.

Katsura, S., H. Ueno, H. Mitsudera, and S. Kouketsu, 2020: Spatial distribution and seasonality of halocline structures in the subarctic North Pacific. *J. Phys. Oceanogr.*, **50**, 95–109, https://doi.org/10.1175/JPO-D-19-0133.1.

Killworth, P. D., D. B. Chelton, and R. A. de Szoeke, 1997: The speed of observed and theoretical long extratropical planetary waves. *J. Phys. Oceanogr.*, **27**, 1946–1966, https://doi.org/10.1175/1520-0485(1997)027<1946:TSOOAT>2.0.CO;2.

Liu, H., S. A. Grodsky, and J. A. Carton, 2009: Observed subseasonal variability of oceanic barrier and compensated layers. *J. Climate*, **22**, 6104–6119, https://doi.org/10.1175/2009JCLI2974.1.

Masson, S., J.-P. Boulanger, C. Menkes, P. Delecluse, and T. Yamagata, 2004: Impact of salinity on the 1997 Indian Ocean dipole event in a numerical experiment. *J. Geophys. Res.*, **109**, C02002, https://doi.org/10.1029/2003JC001807.

Menviel, L., and Coauthors, 2012: Removing the North Pacific halocline: Effects on global climate, ocean circulation and the carbon cycle. *Deep-Sea Res. II*, **61–64**, 106–113, https://doi.org/10.1016/j.dsr2.2011.03.005.

Mignot, J., A. Lazar, and M. Lacarra, 2012: On the formation of barrier layers and associated vertical temperature inversions: A focus on the northwestern tropical Atlantic. *J. Geophys. Res.*, **117**, C02010, https://doi.org/10.1029/2011JC007435.

Mitsudera, H., and Coauthors, 2018: Low ocean-floor rises regulate subpolar sea surface temperature by forming baroclinic jets. *Nat. Commun.*, **9**, 1190, https://doi.org/10.1038/s41467-018-03526-z.

Oka, E., L. D. Talley, and T. Suga, 2007: Temporal variability of winter mixed layer in the mid- to high-latitude North Pacific. *J. Oceanogr.*, **63**, 293–307, https://doi.org/10.1007/s10872-007-0029-2.

——, S. Katsura, H. Inoue, A. Kojima, M. Kitamoto, T. Nakano, and T. Suga, 2017: Long-term change and variation of salinity in the western North Pacific subtropical gyre revealed by 50-year long observations along 137°E. *J. Oceanogr.*, **73**, 479–490, https://doi.org/10.1007/s10872-017-0416-2.

Qiu, B., 2003: Kuroshio extension variability and forcing of the Pacific decadal oscillations: Responses and potential feedback. *J. Phys. Oceanogr.*, **33**, 2465–2482, https://doi.org/10.1175/2459.1.

Roemmich, D., and J. Gilson, 2009: The 2004–2008 mean and annual cycle of temperature, salinity, and steric height in the global ocean from the Argo Program. *Prog. Oceanogr.*, **82**, 81–100, https://doi.org/10.1016/j.pocean.2009.03.004.

Shetye, S. R., A. D. Gouveia, D. Shankar, S. S. C. Shenoi, P. N. Vinayachandran, D. Sundar, G. S. Michael, and G. Nampoothiri, 1996: Hydrography and circulation in the western Bay of Bengal during the northeast monsoon. *J. Geophys. Res.*, **101**, 14 011–14 025, https://doi.org/10.1029/95JC03307.

Sprintall, J., and M. Tomczak, 1992: Evidence of the barrier layer in the surface layer of the tropics. *J. Geophys. Res.*, **97**, 7305–7316, https://doi.org/10.1029/92JC00407.

Talley, L. D., 1985: Ventilation of the subtropical North Pacific: The shallow salinity minimum. *J. Phys. Oceanogr.*, **15**, 633–649, https://doi.org/10.1175/1520-0485(1985)015<0633:VOTSNP>2.0.CO;2.

——, G. L. Pickard, W. J. Emery, and J. H. Swift, 2011: *Descriptive Physical Oceanography: An Introduction*. 6th ed. Academic Press, 564 pp.

Terray, L., L. Corre, S. Cravatte, T. Delcroix, G. Reverdin, and A. Ribes, 2012: Near-surface salinity as nature's rain gauge to detect human influence on the tropical water cycle. *J. Climate*, **25**, 958–977, https://doi.org/10.1175/JCLI-D-10-05025.1.

Tomczak, M., and J. S. Godfrey, 1994: *Regional Oceanography: An Introduction*. Pergamon, 422 pp.

Vallis, G., 2006: The wind- and buoyancy-driven ocean circulation. *Atmospheric and Oceanic Fluid Dynamics: Fundamentals and Large-Scale Circulation*, Cambridge University Press, 667–716, https://doi.org/10.1017/CBO9780511790447.017.

Vialard, J., and P. Delecluse, 1998: An OGCM study for the TOGA decade, Part 2: Barrier-layer formation and variability. *J. Phys. Oceanogr.*, **28**, 1089–1106, https://doi.org/10.1175/1520-0485(1998)028<1089:AOSFTT>2.0.CO;2.

Wallace, J. M., E. M. Rasmusson, T. P. Mitchell, V. E. Kousky, E. S. Sarachik, and H. Von Storch, 1998: On the structure and evolution of ENSO-related climate variability in the tropical Pacific: Lessons from TOGA. *J. Geophys. Res.*, **103**, 14 241–14 259, https://doi.org/10.1029/97JC02905.

Warren, B., 1983: Why is no deep water formed in the North Pacific? *J. Mar. Res.*, **41**, 327–347, https://doi.org/10.1357/002224083788520207.

Waterhouse, A. F., and Coauthors, 2014: Global patterns of diapycnal mixing from measurements of the turbulent dissipation rate. *J. Phys. Oceanogr.*, **44**, 1854–1872, https://doi.org/10.1175/JPO-D-13-0104.1.

Yu, L., 2011: A global relationship between the ocean water cycle and near-surface salinity. *J. Geophys. Res.*, **116**, C10025, https://doi.org/10.1029/2010JC006937.